

Online Monitoring for Neural Network Based Monocular Pedestrian Pose Estimation

Arjun Gupta and Luca Carlone

Abstract—Several autonomy pipelines now have core components that rely on deep learning approaches. While these approaches work well in nominal conditions, they tend to have unexpected and severe failure modes that create concerns when used in safety-critical applications, including self-driving cars. There are several works that aim to characterize the robustness of networks offline, but currently there is a lack of tools to monitor the correctness of network outputs *online* during operation. We investigate the problem of online output monitoring for neural networks that estimate 3D human shapes and poses from images. Our first contribution is to present and evaluate model-based and learning-based monitors for a human-pose-and-shape reconstruction network, and assess their ability to predict the output loss for a given test input. As a second contribution, we introduce an *Adversarially-Trained Online Monitor* (ATOM) that learns how to effectively predict losses from data. ATOM dominates model-based baselines and can detect bad outputs, leading to substantial improvements in human pose output quality. Our final contribution is an extensive experimental evaluation that shows that discarding outputs flagged as incorrect by ATOM improves the average error by 12.5%, and the worst-case error by 126.5%.

I. INTRODUCTION

Neural Networks are growing in popularity due to their ability to find meaningful patterns in high-dimensional data such as camera images. This ability has made them a primary approach in a variety of tasks ranging from natural language processing to vision [1], [2], [3], [4]. While these approaches work well in nominal conditions, they have unexpected and severe failure modes, *e.g.*, when the distribution of the test data significantly differs from training [5], [6]. While many applications can afford occasional failures (*e.g.*, AR/VR, domestic robotics), incorrect predictions may have disastrous consequences in safety-critical applications: in May 2017, a Tesla Model S was involved in a fatal accident in which the autopilot system did not detect a tractor-trailer [7], [8]; in March 2018, a self-driving Uber vehicle failed to detect a pedestrian and provide a timely warning to the emergency backup driver, killing a woman in Arizona [9].

While neural networks are powerful, there are no good ways to bound their error for an unseen datapoint, especially one unlike those from training or validation. To mitigate this problem, many recent papers attempt to verify the correctness or stability of neural network outputs with respect to specific inputs. A variety of methods have already been developed



Fig. 1. 3D human shape and pose estimation networks are prone to making mistakes when tested outside the training distribution. We discuss how to detect failures and propose an *Adversarially-Trained Online Monitor* (ATOM) to detect incorrect outputs. Human pose estimation is crucial for safety-critical applications, including pedestrian detection.

for offline verification [10], [11], [12], [13]; however, these methods are limited in the size of the network, type of network, or only find adversarial examples without explicitly bounding the performance in all cases. These limitations make the existing methods hardly useful for modern day, large-scale machine learning which uses large, complex networks. A new set of works attempts to monitor network outputs at runtime to quantify their reliability. Among these, the works [14], [15] rely on hand-crafted constraints and time-series input data for monitoring object detection pipelines. Other works explore learning-based approaches for neural network monitoring. These approaches range from learning how to predict the correctness of segmentation masks for medical imaging [16] to false negative detection for road-sign detection [17].

In this paper, we propose the first approach to monitor the quality of 3D human pose estimates from a neural network. Human pose estimation is crucial for pedestrian detection in intelligent transportation, as well as in safety-critical applications of robotics (*e.g.*, collaborative manufacturing). We develop several model-based monitors to detect incorrect human pose predictions. We also employ a pre-trained 2D human segmentation network to monitor the 3D network outputs. As a second contribution, we develop an *Adversarially-Trained Online Monitor* (ATOM), which is trained end-to-end to predict losses on the 3D human (shape and) pose outputs. A depiction of the overall structure of ATOM for 3D human pose monitoring is shown in Fig. 2. Finally, we provide an extensive experimental evaluation across four benchmarking datasets. Our results show that, due to the complexity of the problem, model-based approaches have limited success at monitoring the network outputs. Learning-based approaches provide a significant improvement over model-based methods and ATOM dominates the compared techniques.

In summary, we propose three key contributions:

- 1) We develop and implement several baseline methods for loss prediction and online monitoring of 3D human

A. Gupta and L. Carlone are with the Laboratory for Information & Decision Systems, Massachusetts Institute of Technology, Cambridge, MA, USA. {argupta, lcarlone}@mit.edu

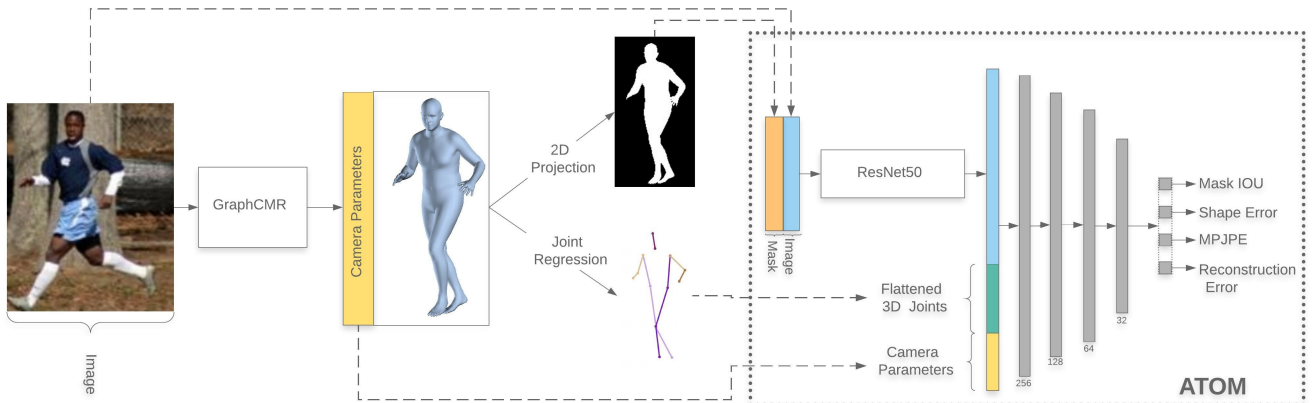


Fig. 2. We propose ATOM, a learning-based approach to monitor the outputs of a 3D human shape and pose estimation network (GraphCMR [18]). At test time, ATOM takes as input the original input image, the 2D projection of the 3D mesh produced by GraphCMR, camera parameters output by GraphCMR, and 3D joints extracted from the 3D mesh. It then predicts the quality (*i.e.*, the loss) of the provided mesh model.

pose estimates. These baselines include both model-based and learning-based methods leveraging existing networks;

- 2) We develop a new architecture, named *Adversarially-Trained Online Monitor* (ATOM), to directly predict different losses of the estimated 3D human pose outputs.
- 3) We present an extensive experimental evaluation that shows that learning-based monitors are extremely effective in predicting the output loss and at detecting bad network predictions.

In the following, we review related work (Section II) and present several baseline techniques for output monitoring (Section III). Then, we introduce ATOM as a more effective learning-based monitor (Section IV). Finally, we present the results of our experimental analysis (Section V) and draw conclusions (Section VI).

II. RELATED WORK

We review related work dealing with network verification and monitoring and refer the reader to [10], [11] for a more extensive survey. Seshia *et al.* [19] provide an excellent overview of why verifying neural networks is much more difficult than verifying other types of programs and outline the technical advances necessary to verify them.

A. Offline Verification

1) *Reachability Analysis*: A common approach for neural network verification is to analyze the *reachable set*, *i.e.*, the set of possible network outputs for a given set of inputs, to assess when the network outputs unsafe values [12], [13], [20]. Katz *et al.* [21] uses an SMT solver to ensure that under certain preconditions, the outputs of the neural network obey a set of constraints. Fazlyab *et al.* [22] abstract activation functions in the form of quadratic constraints and solve the resulting semidefinite program to find the reachable output set of a network. Contrarily to offline verification, our goal is to verify the network outputs during operation.

2) *Adversarial Perturbations*: Another major approach for quantifying the robustness of a network is to find the minimum *adversarial perturbation* that causes the network to make significant errors. Bastani *et al.* [23], Cheng *et al.* [24], and Sun *et al.* [25] attempt to find the adversarial perturbation with minimum norm that causes a network to misclassify examples. Huang *et al.* [26] guarantee that they find an adversarial example (if it exists) for a network to a particular class of perturbation. AI2 [27] attempts to solve problems of scalability and precision for perturbation analysis by using the theory of abstract interpretation to capture all variations of a perturbation at once. Kolter *et al.* [28] learn a classifier that is robust to any norm-bounded adversarial attack. DeepXplore [29], and DeepGauge [30] find adversarial examples by perturbing images to maximize neuron coverage and cause the network to misclassify examples. Sun *et al.* [31] discover adversarial perturbations using a concolic testing paradigm that alternates between concrete and symbolic execution to generate adversarial examples. Dvijotham *et al.* [32] formulate adversarial perturbations as an optimization problem and approximate the dual to get an upper bound on the adversarial error rate. Wong *et al.* [33] attempt to scale the process of making networks robust to adversarial examples to deep learning architectures.

3) *Test Case Generation*: The above methods all test the network by finding some simple perturbation (*e.g.*, additive pixel-wise noise) of an existing image that the network fails to identify correctly. However, this is limited in scope, and it doesn't guarantee correctness on images that have large, structural dissimilarity to the training data. Some recent papers have identified other solutions to verifying networks against more structured and realistic perturbations. DeepTest [34] automatically modifies images for self-driving in a structured way (*e.g.*, by adding rain, fog) and searches for input images that maximize the network neuron coverage. Fremont *et al.* [35], and Cumhur *et al.* [36] develop frameworks to specify arbitrary, randomized scenarios for autonomous driving and generate photo-realistic images for testing and training networks. While these pipelines are able

to synthesize completely new images, they both require the user to manually specify test cases, implicitly reducing their ability to find bad samples.

B. Online Monitoring

1) *Temporal Logic*: Balakrishnan *et al.* [14] use Timed Quality Temporal Logic (TQTL) to reason about logical relations between boolean-value propositions on the network output over time. Kang *et al.* [15] present the idea of model assertions, which similarly place a constraint on the model outputs to detect when they violate certain conditions. These approaches add constraints on the network outputs, but require hand-made boolean constraints. Moreover, they require the network to predict over several timesteps before providing a feedback.

2) *Learning-based Monitoring*: Learning-based monitoring is most closely related to our proposal. DeVries *et al.* [16] develop a method for verifying a semantic segmentation network for medical imaging by passing the original image, the segmentation, and a confidence mask to an external verification network. Hecker *et al.* [37] create a pipeline to predict whether an autonomous driving system will make bad predictions in the future. Saxena *et al.* [38] and Daftry *et al.* [39] develop a network to verify collision-free trajectories for a vision-based drone platform. Rahman *et al.* [17] process the hidden layer outputs of a neural network to predict when a traffic sign detection network outputs false negatives. Cheng *et al.* [40] and Henzinger *et al.* [41] observe neuron activation patterns to monitor when the network is operating on inputs unlike the data seen during training. Hendrycks *et al.* [5] develop a method of monitoring network confidence based on softmax probabilities. Our model works on networks without softmax activations, and gives finer-grained monitoring information (*i.e.*, we predict the future loss for a given input). In addition, none of these works tackle the problem of monitoring 3D human pose estimates, which is key to autonomous vehicles.

III. ONLINE MONITORING OF 3D HUMAN POSES: PROBLEM STATEMENT AND BASELINE APPROACHES

A. Problem Statement

We address the problem of monitoring GraphCMR [18], a state-of-the-art human shape and pose reconstruction network. GraphCMR takes images as input and outputs the SMPL mesh [42] of the center-most human. More practically, we solve the problem of detecting when the SMPL mesh output from GraphCMR does not align with the input image. Our approach is to design a monitor that provides a score of mesh correctness based on how it compares to the input image. We then use those scores to detect when a mesh might be incorrect. Before we proceed with our contributions, we first define the language used throughout the section:

1) *Skinned Multi-Person Linear Model (SMPL)*: We make frequent references to SMPL [42], the output of GraphCMR. SMPL parametrizes a full human mesh using a set of pose parameters, Θ , which define the relative angle-axis rotation between joints and a set of body-shape parameters β , which

describe the way the human appears. From an SMPL model, we can also regress the 3D human joint-locations, which we use in our monitoring approaches.

2) *Human Shape and Pose Estimation*: GraphCMR is an example of a human-shape-and-pose estimation approach, which fits an SMPL mesh to a monocular image. Previous human shape and pose estimation techniques include SMPLfy [43], HMR [44], NBF [45], as well as many others [46], [47], [48], [49], [50]. We design a monitor for GraphCMR because it provides state-of-the-art performance, although it still fails on more difficult input instances.

We proceed by describing our baseline approaches for human pose monitoring, including approaches that use existing neural network models.

B. Feature Matching (FeatureM)

Our first approach projects the estimated 3D mesh into a 2D binary mask using Neural 3D Mesh Renderer [51] and compares it to the original image using feature extraction and matching (Fig. 3). Classically, SIFT [52], SURF [53], and ORB [54] are commonly used for object detection in cluttered images. We adapt ORB to detect features for our monitoring application. While ORB features work well when comparing two RGB images, they fail when comparing an RGB image with a binary mask. To resolve this issue, we first extract contours using the Canny detector [55] for both the RGB image and the binary mask and then perform feature detection and matching on the contours.

We match keypoints from the binary mask to the two nearest keypoints in the RGB image based on feature descriptors. Because the mask and the original image should have the human at the same location, we additionally use the pixel distance between keypoints to determine inlier matches. We count a match as an inlier if the descriptor distance to the matched keypoint is less than 0.75 times the descriptor distance to the next closest keypoint and the keypoints are within 26 pixels of each other (determined experimentally). We score the image correctness based on the percentage of keypoints in the 2D binary mask that correspond to features in the original RGB image. Fig. 3 shows that this approach, that we denote as FeatureM, picks out joints along the silhouette (the most feature-rich regions) and uses the corresponding mismatch to compute an error score.

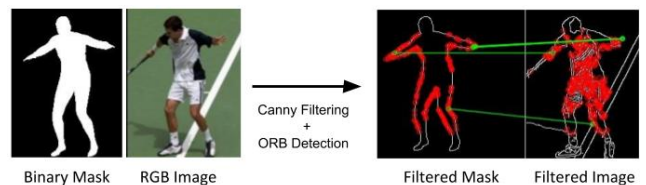


Fig. 3. FeatureM performs edge detection on a given RGB image and on the binary mask obtained by projecting the 3D mesh by GraphCMR. It then compares features in the edge images to assess the mesh quality. The red circles are all detected features, and the green circles are the features that are considered inlier matches.

C. Canny Edge Matching (CannyM)

Our second monitoring baseline is based on the Canny edge detector. The approach, named CannyM, is motivated by the observation that the 2D projection of the human mesh should precisely outline the human silhouette in the image. We once again apply Canny filtering to both the binary mask and the original RGB image to get contours. We then dilate the contours from the original input image using a fixed size kernel (a 5×5 kernel in our tests) and measure the percentage of the contour points from the 2D human binary mask that overlap with a dilated contour from the RGB image. The percentage overlap is used as score by the monitoring approach.

D. Shape and Pose Consistency (TimeM)

For timeseries data, a clear baseline is to judge the consistency of predictions over time. These consistency metrics are similar in spirit to TQTL [14] where we reason about the consistency of the relationship between consecutive pose predictions. We assume that we can correctly re-identify the same human across multiple images: the datasets we use for evaluation provide an ID for each annotated human.¹ This third baseline approach, named TimeM, is applied independently to each ID, and leverages the loss functions proposed by Kim *et al.* [57].

The TimeM score is the sum of two terms: *shape consistency* and *pose consistency*. *Shape consistency* enforces the observation that the body shape of a person is constant over time. *Pose consistency* ensures that the difference between consecutive poses corresponds to a feasible human motion. We formalize shape and pose consistency below.

a) Shape Consistency: For shape consistency, we maintain a database of the average body shape seen for each person ID. Each time we observe the same ID, we compute the difference between the predicted body-shape parameters and the stored average for that ID to get a similarity score. We update the average for future use by averaging the new detection body shape with the current average. Shape Consistency evaluates the correctness of a mesh based on its deviation from the average body shape for that subject. The shape consistency metric is defined as:

$$\mathcal{L}_{sc} = \|\beta_t - \beta_{avg}\|_F^2 \quad (1)$$

Where β_t is a matrix of the body shape parameters for the detection at time t and the β_{avg} is a matrix of the average body shape for that ID. The symbol $\|\cdot\|_F$ denotes the Frobenius norm.

b) Pose Consistency: Unlike shape consistency, pose consistency is measured between adjacent predictions only and captures the change in pose due to joint movements. To measure pose consistency, we measure the distance between corresponding 3D joints in the current and previous timestep. We weight each joint error based on its distance from the core body (e.g. an elbow cannot move as quickly as a hand) to

reduce the larger errors from more distant appendage points. We additionally include a history buffer which compares the current pose against previous poses from a number of timesteps back in the case that the previous errors were high. This ensures that a bad prediction in a sequence of poses does not cause future good predictions to have high error. We formalize this below:

$$\mathcal{L}_{pc} = \min_{0 \leq i \leq h} (J_{t-i} - J_t)^T W (J_{t-i} - J_t) \quad (2)$$

Where h is the history length, J_t are the joints observed at time t , and W is a diagonal matrix of joint weights. The loss can be thought of as enforcing a prior that humans tend to have very small changes between consecutive poses.

TimeM scores each output using the overall score $\mathcal{L}_{sc} + \mathcal{L}_{pc}$. Since we do not know all the detections of each person ID beforehand, the first time we encounter a new ID, we give them a 0 score since we have no prior experience to use to compute the scores (1)-(2). As we observe more instances of the ID, we increase our ability to discern good predictions from bad.

E. MaskRCNN Intersection Over Union (MRcnnM)

The above approaches use purely classical model-based methods to monitor the 3D human meshes produced by GraphCMR; as we will see, these techniques perform poorly in practice. The first two approaches (FeatureM and CannyM) tend to fail on images with cluttered backgrounds, where edge detection returns contours where the human is difficult to distinguish. TimeM, on the other hand, does not apply when there is no prediction history. This section solves these issues by leveraging a learning-based 2D pixel-wise segmentation network (we use MaskRCNN [58]) to detect failures in 3D human mesh outputs by GraphCMR.

This monitoring approach, named MRcnnM, uses the predicted mask from MaskRCNN as a pseudo ground-truth to verify the correctness of binary mask obtained from GraphCMR. We compute the score for a GraphCMR output as the Intersection over Union of the MaskRCNN mask and the binary mask obtained by projecting the 3D mesh:

$$\mathcal{L}_{IOU} = \frac{2}{|M_m| + |M_p|} \sum_{(i,j) \in M_p} \mathbb{I}\{M_p(i,j) = M_m(i,j)\} \quad (3)$$

Where M_m is the mask produced by MaskRCNN, M_p is the predicted mask, (i,j) are pixel coordinates, and \mathbb{I} is the indicator function which is 1 when $M_p(i,j) = M_m(i,j)$ and zero otherwise. Because there could be potentially many humans, and the mesh prediction network only predicts one, we choose the highest IOU score.

At a first glance, using a neural network to monitor the correctness of another network seems circular, as the monitor network itself is bound to be unreliable. However, the results show that this is in fact a much more effective method than the classical approaches. The intuition is that training MaskRCNN is much easier than training GraphCMR, since the former only requires labeling a 2D image (relatively easy for

¹In practice, data association would be based on temporal tracking [56].

a human), while the latter requires training on 3D meshes, which are difficult to label at scale. Therefore, MaskRCNN has access to a much larger training set which allows it to perform well on instances that cause failures in GraphCMR.

While the MRcnnM approach can successfully solve the problems faced by the model-based approaches, it is still unreliable when monitoring the worst samples (as seen in Section V-D). In addition, MRcnnM is unable to accurately predict losses on the SMPL pose, a critical metric for correctness. This motivates us to design a novel approach, ATOM, presented below.

IV. ATOM: ADVERSARIALLY-TRAINED ONLINE MONITOR

While the previous monitors made use of model-based approaches or existing neural networks, ATOM is taught end-to-end to predict losses on GraphCMR outputs. Our network takes as input: (i) a greyscale version of the original RGB image concatenated with the binary mask of the predicted mesh, (ii) the 3D joint locations, and (iii) the camera parameters output by GraphCMR. ATOM simultaneously outputs the predicted *MaskIOU* between the binary mask and a theoretical ground-truth mask, the *Mean Per Joint Prediction Error* (MPJPE) [59], the *Reconstruction Error* (REC) [59], and *Shape Error* which is the per-vertex error of the output mesh.

1) *Network Architecture*: We depict our model architecture in Fig. 2. We concatenate the greyscale image and the binary mask along the channel axis and use a Resnet50 architecture to encode their combination. We remove the last layer and use the final encoded vector through the rest of the network. We separately flatten the 3D joint locations and concatenate them with the encoded image and the camera parameters. We pass the concatenated vector through a set of fully-connected layers to regress the loss on GraphCMR outputs. Notice that our model architecture is relatively shallow for the deep learning era. This allows it to run at 10 Hz on a modest GPU, meaning that it can reasonably be run alongside another network and give real time feedback at low computational cost.

2) *Loss Functions*: For training loss, we use the Mean Squared Error (MSE) between the network output and the ground-truth:

$$\mathcal{L}_{\text{mse}} = \frac{1}{n} \sum_i (\hat{y}_i - y_i)^2 \quad (4)$$

Where \hat{y}_i is the prediction of ATOM for the i^{th} data-point, y_i is the ground-truth loss for that mesh, and n is the number of samples.

3) *Mesh Augmentation for Learning Approaches*: Because we only monitor the correctness of labels, we can dramatically increase our training data by perturbing GraphCMR outputs to get new loss labels. SMPL meshes can easily be perturbed by perturbing the mesh parameters. This makes data augmentation simple and quite robust. During training, we randomly perturb a batch of meshes with a predetermined probability (0.6 for the model reported in the results)

by adding Gaussian noise to the body-shape and pose-parameters of the predicted mesh. We observe that this leads to a significant improvement in out-of-sample monitoring.

V. EXPERIMENTS

We present a three-part evaluation of the baseline monitors and ATOM. Section V-B demonstrates that we can effectively predict output error metrics for GraphCMR. Section V-C justifies our architecture and the effect of data augmentation via an ablation study. Finally, Section V-D describes the use of ATOM for monitoring GraphCMR outputs with quantitative and qualitative results. Before the evaluation, we describe our datasets and evaluation metrics.

A. Datasets and Evaluation Metrics

The human mesh prediction model [18] is evaluated on three datasets: Leeds Sports Poses (LSP) [60], Unite the People (UP-3D) [61], and Human3.6M [62]. Each dataset has its own set of evaluation metrics. LSP uses *Mask Accuracy* with annotation from the UP dataset, UP-3D uses *Shape Error*, and Human3.6M uses *MPJPE* and *REC* (see section IV) to evaluate model performance. We add an additional dataset, PedX [57], for an out-of-distribution comparison, and evaluate the projected 2D masks on this dataset as well. We use *Mask IOU* (as defined in Section III-E) instead of *Mask Accuracy* because it is more consistent across LSP and PedX, and it more accurately captures mask correctness since it does not consider free-space pixels.

We train ATOM exclusively on the test set for GraphCMR. We use the first 50% of test data for training, 10% for validation, and evaluate on the remaining 40%. We do not train on PedX and use all of PedX for evaluation.

B. Loss Prediction

We first evaluate the monitors discussed in this paper by reporting how their predicted loss (for a given input) correlates with the actual loss, computed using the ground truth labels.

TABLE I
LOSS CORRELATION ON LSP, UP-3D, HUMAN3.6M, AND PEDX

Method	UP-3d	LSP	Human3.6M		PedX
	Shape	Mask IOU	MPJPE	REC	Mask IOU
FeatureM	0.08	0.09	0.17	0.19	0.16
CannyM	0.11	0.51	0.19	0.21	0.20
TimeM	n/a	n/a	0.19	0.17	0.09
MRcnnM	0.29	0.75	0.28	0.21	0.80
ATOM	0.46	0.85	0.67	0.69	0.75

Table I shows that the model-based approaches produce scores that are minimally correlated with the ground-truth losses. FeatureM has exceptionally low correlations, likely because of the many failure modes of the feature detector in cluttered images. CannyM stands out with non-trivial correlation on LSP where the humans tend to be higher-resolution and better contrasted with the background (allowing cleaner human edge extraction). The performance drops significantly on PedX, likely due to reduced resolution and contrast in the

PedX data and background clutter from the industrial setting. CannyM clearly beats FeatureM on all tasks, which is expected because FeatureM has the exact same failure modes as CannyM (when human edges are indistinguishable from background clutter) with the additional failure mode from bad feature detections. TimeM performs reasonably when predicting the pose errors, as expected since it computes pose consistency, but it fails to predict the less directly related MaskIOU metric for PedX. Moreover, TimeM cannot be applied to UP-3D or LSP because they are not timeseries.

Table I also shows that MRcnnM exhibits a substantially higher correlation score. MRcnnM is the first approach, among the ones discussed in this paper, that accurately predicts loss. It even beats ATOM on PedX, although we later show that ATOM is much more effective at detecting the worst predictions for PedX. In addition, notice that all baseline methods, including MRcnnM, are unable to predict the pose or shape metrics because they either do not have the information to judge these losses (MRcnnM, CannyM, FeatureM), or they can only compare predictions over time without reference to the original image (TimeM).

On the other hand, ATOM is able to generate losses that are very strongly correlated with the ground-truth losses. The correlation is lower for *Shape Error*: this is expected since *Shape Error* depends on the location of individual vertices in the mesh, which ATOM does not have access to. However, the network is able to get high correlations with the pose error metrics (*MPJPE* and *REC*) on Human3.6M, a key metric for pedestrian detection monitoring, where the pose is more important than the shape of the human.

C. Ablation Study

In this section, we systematically remove key components of ATOM and see that each design choice has an immediate effect at improving network correctness. The model names and their corresponding features are listed below:

- (i) noAug: ATOM without augmentation during training.
- (ii) noJoint: ATOM without 3D joint inputs.
- (iii) noMask: ATOM without binary mask inputs.

TABLE II
ABLATION STUDY: LOSS CORRELATION FOR ATOM

Method	UP-3d Shape	LSP Mask IOU	Human3.6M		PedX Mask IOU
			MPJPE	Rec.	
ATOM	0.46	0.85	0.67	0.69	0.75
noAug	0.46	0.69	0.67	0.67	0.46
noMask	0.33	0.443	0.56	0.57	-0.033
noJoint	0.44	0.791	0.69	0.67	0.606

Table II shows that the segmentation mask input is integral for predicting any of the metrics successfully as shown by the noMask performance. The augmentation and joints drastically improve the out-of-sample correlation with PedX as well as many of the key in-sample performance indicators.

D. Monitoring: Results and Timing

We now present results produced by ATOM and baseline methods when monitoring GraphCMR. We show the effect of

monitoring by removing outputs that are in the worst 20% of scores (losses) computed by our monitoring methods, and we enumerate the percent improvement for each evaluation metric. In other words, we evaluate how the error metrics of GraphCMR improve when rejecting bad outputs as detected by each monitor.

Table III shows the percentage improvement in the average error (“avg” in Table III) and the worst-case error (“min” or “max”, depending on the metric, in Table III) for each of the discussed monitors. The table shows that ATOM is able to significantly improve the average error metrics by up to 12.5%. ATOM is also able to consistently improve the error value for the worst sample, improving the minimum MaskIOU on PedX by 126.5%. MaskRCNN does provide some marginally better improvements in PedX and UP-3D; however, it is extremely inconsistent and cannot reduce the worst values for LSP or PedX.

In addition to having the ability to effectively monitor predictions, ATOM’s small architecture allows it to be run in real time. The last column in Table III shows that ATOM can run in milliseconds on a 1060 Geforce Mobile GPU. This observation suggests that ATOM can be effectively used for online monitoring since it does not add a significant computational burden.

Fig. 4 provides a visualization of the outputs deemed incorrect by ATOM. In particular, the figure shows the worst predictions on the LSP test set and the corresponding worst predictions after rejecting bad outputs using ATOM. We provide the MaskIOU score for the prediction under each image. Notice that the original predictions include several examples where the mesh is completely misaligned with the actual human and frequently the mesh is not facing the correct direction, an important factor for determining where a human may move next. On the other hand, after monitoring and removal, all predictions have significantly higher score and match the provided image with a visibly correct body orientation and pose.

VI. CONCLUSION

In this paper, we discussed techniques for monitoring a 3D human pose and shape reconstruction network. We demonstrated several model-based approaches, and showed that they cannot effectively predict the loss or detect bad outputs. We found that networks that predict a simpler form of output (either directly the loss or the 2D segmentation mask) can effectively monitor a network with more complex, 3D, outputs. We developed a monitoring network, ATOM, that dominates the baseline approaches in terms of accuracy and runtime. In future work, we plan to explore the use of Graph Convolutional Networks as an alternative architecture and apply ATOM as a weak supervisor to improve the performance of GraphCMR. As systems become more advanced and need to interact with humans, accurate monitoring of human detections and pose estimation becomes a prerequisite for safety-critical applications, and ATOM provides the first example of online 3D monitoring for these applications.

TABLE III
% PERFORMANCE INCREASE AFTER PRUNING OUTPUTS WITH HIGH PREDICTED LOSS ON LSP, UP-3D, HUMAN3.6M, AND PEDX

Method	UP-3D Shape		LSP Mask IOU		Human3.6M MPJPE			PedX Mask IOU		Average Prediction Time (s)	
	avg ↓	max ↓	avg ↑	min ↑	avg ↓	max ↓	avg ↓	max ↓	avg ↑		min ↑
FeatureM	0.0%	0.0%	0.4%	25.6%	2.5%	0.0%	3.6%	0.0%	0.4%	1.2%	0.012
CannyM	4.2%	0.0%	2.3%	0.0%	2.4%	0.0%	3.6%	0.0%	0.5%	0.0%	0.43
TimeM	-	-	-	-	3.7%	0.0%	3.6%	0.0%	0.5%	0.0%	0.0015
MRcnnM	12.5%	21.9%	3.7%	25.6%	4.9%	53.4%	5.4%	26.1%	3.5%	0.0%	1.25
ATOM	10.4%	21.9%	3.7%	87.5%	11.1%	70.0%	12.5%	26.1%	3.4%	126.5%	0.0086



Fig. 4. We visualize the GraphCMR outputs with the worst losses on LSP and the corresponding worst outputs in the set after applying ATOM monitoring and removal. The Mask IOU score for each prediction is noted under the image.

REFERENCES

- [1] A. Garcia-Garcia, S. Orts-Escolano, S. Oprea, V. Villena-Martinez, and J. García-Rodríguez, "A review on deep learning techniques applied to semantic segmentation," *ArXiv Preprint: 1704.06857*, 2017.
- [2] K. He, X. Zhang, S. Ren, and J. Sun, "Deep residual learning for image recognition," pp. 770–778, 2016.
- [3] J. Devlin, M.-W. Chang, K. Lee, and K. Toutanova, "Bert: Pre-training of deep bidirectional transformers for language understanding," *arXiv preprint arXiv:1810.04805*, 2018.
- [4] Z. Zou, Z. Shi, Y. Guo, and J. Ye, "Object detection in 20 years: A survey," *arXiv preprint arXiv:1905.05055*.
- [5] D. Hendrycks and K. Gimpel, "A baseline for detecting misclassified and out-of-distribution examples in neural networks," *ArXiv*, vol. abs/1610.02136, 2016.
- [6] S. Liang, Y. Li, and R. Srikant, "Enhancing the reliability of out-of-distribution image detection in neural networks," *arXiv preprint arXiv:1706.02690*, 2017.
- [7] T. Guardian, "Tesla driver dies in first fatal crash while using autopilot mode," www.theguardian.com/technology/2016/jun/30/tesla-autopilot-death-self-driving-car-elon-musk, 2016.
- [8] I. Spectrum, "Fatal tesla self-driving car crash reminds us that robots aren't perfect," <https://spectrum.ieee.org/cars-that-think/transportation/self-driving/fatal-tesla-autopilot-crash-reminds-us-that-robots-arent-perfect>, 2017.
- [9] T. N. Y. Times, "Self-Driving Uber Car Kills Pedestrian in Arizona, Where Robots Roam," <https://www.nytimes.com/2018/03/19/technology/uber-driverless-fatality.html>, 2018.
- [10] W. Xiang, P. Musau, A. A. Wild, D. M. Lopez, N. Hamilton, X. Yang, J. A. Rosenfeld, and T. T. Johnson, "Verification for machine learning, autonomy, and neural networks survey," *CoRR*, vol. abs/1810.01989, 2018. [Online]. Available: <http://arxiv.org/abs/1810.01989>
- [11] F. Leofante, N. Narodytka, L. Pulina, and A. Tacchella, "Automated verification of neural networks: Advances, challenges and perspectives," *CoRR*, vol. abs/1805.09938, 2018. [Online]. Available: <http://arxiv.org/abs/1805.09938>
- [12] W. Xiang, H. Tran, and T. T. Johnson, "Reachable set computation and safety verification for neural networks with relu activations," *CoRR*, vol. abs/1712.08163, 2017. [Online]. Available: <http://arxiv.org/abs/1712.08163>
- [13] A. Lomuscio and L. Maganti, "An approach to reachability analysis for feed-forward relu neural networks," *CoRR*, vol. abs/1706.07351, 2017. [Online]. Available: <http://arxiv.org/abs/1706.07351>
- [14] A. Balakrishnan, A. G. Puranic, X. Qin, A. Dokhanchi, J. V. Deshmukh, H. Ben Amor, and G. Fainekos, "Specifying and evaluating quality metrics for vision-based perception systems," in *2019 Design, Automation Test in Europe Conference Exhibition (DATE)*, March 2019, pp. 1433–1438.
- [15] D. Kang, D. Raghavan, P. Bailis, and M. Zaharia, "Model assertions for debugging machine learning," 2018.
- [16] T. DeVries and G. W. Taylor, "Leveraging uncertainty estimates for predicting segmentation quality," *CoRR*, vol. abs/1807.00502, 2018. [Online]. Available: <http://arxiv.org/abs/1807.00502>
- [17] Q. M. Rahman, N. Sünderhauf, and F. Dayoub, "Did you miss the sign? A false negative alarm system for traffic sign detectors," *CoRR*, vol. abs/1903.06391, 2019. [Online]. Available: <http://arxiv.org/abs/1903.06391>
- [18] N. Kolotouros, G. Pavlakos, and K. Daniilidis, "Convolutional mesh regression for single-image human shape reconstruction," in *IEEE Conf. on Computer Vision and Pattern Recognition (CVPR)*, 2019.
- [19] S. A. Seshia and D. Sadigh, "Towards verified artificial intelligence," *CoRR*, vol. abs/1606.08514, 2016. [Online]. Available: <http://arxiv.org/abs/1606.08514>
- [20] W. Xiang, H. Tran, and T. T. Johnson, "Output reachable set estimation and verification for multi-layer neural networks," *CoRR*, vol. abs/1708.03322, 2017. [Online]. Available: <http://arxiv.org/abs/1708.03322>
- [21] G. Katz, C. W. Barrett, D. L. Dill, K. Julian, and M. J. Kochenderfer, "Reluplex: An efficient SMT solver for verifying deep neural networks," *CoRR*, vol. abs/1702.01135, 2017. [Online]. Available: <http://arxiv.org/abs/1702.01135>
- [22] M. Fazlyab, M. Morari, and G. Pappas, "Safety verification and robustness analysis of neural networks via quadratic constraints and semidefinite programming," *ArXiv*, vol. abs/1903.01287, 2019.
- [23] O. Bastani, Y. Ioannou, L. Lampropoulos, D. Vytiniotis, A. V. Nori, and A. Criminisi, "Measuring neural net robustness with constraints," *CoRR*, vol. abs/1605.07262, 2016. [Online]. Available: <http://arxiv.org/abs/1605.07262>

- [24] C. Cheng, G. Nührenberg, and H. Ruess, "Maximum resilience of artificial neural networks," *CoRR*, vol. abs/1705.01040, 2017. [Online]. Available: <http://arxiv.org/abs/1705.01040>
- [25] Y. Sun, X. Huang, and D. Kroening, "Testing deep neural networks," *CoRR*, vol. abs/1803.04792, 2018. [Online]. Available: <http://arxiv.org/abs/1803.04792>
- [26] X. Huang, M. Kwiatkowska, S. Wang, and M. Wu, "Safety verification of deep neural networks," *CoRR*, vol. abs/1610.06940, 2016. [Online]. Available: <http://arxiv.org/abs/1610.06940>
- [27] T. Gehr, M. Mirman, D. Drachler-Cohen, P. Tsankov, S. Chaudhuri, and M. Vechev, "Ai2: Safety and robustness certification of neural networks with abstract interpretation," in *2018 IEEE Symposium on Security and Privacy (SP)*, May 2018, pp. 3–18.
- [28] J. Z. Kolter and E. Wong, "Provable defenses against adversarial examples via the convex outer adversarial polytope," *arXiv preprint arXiv:1711.00851*, vol. 1, no. 2, p. 3, 2017.
- [29] K. Pei, Y. Cao, J. Yang, and S. Jana, "Deepxplore: Automated whitebox testing of deep learning systems," *CoRR*, vol. abs/1705.06640, 2017. [Online]. Available: <http://arxiv.org/abs/1705.06640>
- [30] L. Ma, F. Juefei-Xu, J. Sun, C. Chen, T. Su, F. Zhang, M. Xue, B. Li, L. Li, Y. Liu, J. Zhao, and Y. Wang, "Deepgauge: Comprehensive and multi-granularity testing criteria for gauging the robustness of deep learning systems," *CoRR*, vol. abs/1803.07519, 2018. [Online]. Available: <http://arxiv.org/abs/1803.07519>
- [31] Y. Sun, M. Wu, W. Ruan, X. Huang, M. Kwiatkowska, and D. Kroening, "Concolic testing for deep neural networks," *CoRR*, vol. abs/1805.00089, 2018. [Online]. Available: <http://arxiv.org/abs/1805.00089>
- [32] K. Dvijotham, R. Stanforth, S. Gowal, T. A. Mann, and P. Kohli, "A dual approach to scalable verification of deep networks," *CoRR*, vol. abs/1803.06567, 2018. [Online]. Available: <http://arxiv.org/abs/1803.06567>
- [33] E. Wong, F. Schmidt, J. H. Metzen, and J. Z. Kolter, "Scaling provable adversarial defenses," in *Advances in Neural Information Processing Systems 31*, S. Bengio, H. Wallach, H. Larochelle, K. Grauman, N. Cesa-Bianchi, and R. Garnett, Eds. Curran Associates, Inc., 2018, pp. 8400–8409. [Online]. Available: <http://papers.nips.cc/paper/8060-scaling-provable-adversarial-defenses.pdf>
- [34] Y. Tian, K. Pei, S. Jana, and B. Ray, "Deepest: Automated testing of deep-neural-network-driven autonomous cars," *CoRR*, vol. abs/1708.08559, 2017. [Online]. Available: <http://arxiv.org/abs/1708.08559>
- [35] D. J. Fremont, X. Yue, T. Dreossi, S. Ghosh, A. L. Sangiovanni-Vincentelli, and S. A. Seshia, "Scenic: Language-based scene generation," *CoRR*, vol. abs/1809.09310, 2018. [Online]. Available: <http://arxiv.org/abs/1809.09310>
- [36] C. E. Tuncali, G. E. Fainekos, H. Ito, and J. Kapinski, "Simulation-based adversarial test generation for autonomous vehicles with machine learning components," *CoRR*, vol. abs/1804.06760, 2018. [Online]. Available: <http://arxiv.org/abs/1804.06760>
- [37] S. Hecker, D. Dai, and L. V. Gool, "Failure prediction for autonomous driving," *CoRR*, vol. abs/1805.01811, 2018. [Online]. Available: <http://arxiv.org/abs/1805.01811>
- [38] D. M. Saxena, V. Kurtz, and M. Hebert, "Learning robust failure response for autonomous vision based flight," in *2017 IEEE International Conference on Robotics and Automation (ICRA)*, May 2017, pp. 5824–5829.
- [39] S. Daffry, S. Zeng, J. A. Bagnell, and M. Hebert, "Introspective perception: Learning to predict failures in vision systems," *CoRR*, vol. abs/1607.08665, 2016. [Online]. Available: <http://arxiv.org/abs/1607.08665>
- [40] C.-H. Cheng, G. Nührenberg, and H. Yasuoka, "Runtime monitoring neuron activation patterns," *2019 Design, Automation and Test in Europe Conference and Exhibition (DATE)*, pp. 300–303, 2018.
- [41] T. A. Henzinger, A. Lukina, and C. Schilling, "Outside the box: Abstraction-based monitoring of neural networks," *arXiv preprint arXiv:1911.09032*, 2019.
- [42] M. Loper, N. Mahmood, J. Romero, G. Pons-Moll, and M. J. Black, "SMPL: A skinned multi-person linear model," *ACM Trans. Graphics (Proc. SIGGRAPH Asia)*, vol. 34, no. 6, pp. 248:1–248:16, Oct. 2015.
- [43] F. Bogo, A. Kanazawa, C. Lassner, P. Gehler, J. Romero, and M. J. Black, "Keep it SMPL: Automatic estimation of 3d human pose and shape from a single image," in *European Conf. on Computer Vision (ECCV)*, B. Leibe, J. Matas, N. Sebe, and M. Welling, Eds., 2016.
- [44] A. Kanazawa, M. J. Black, D. W. Jacobs, and J. Malik, "End-to-end recovery of human shape and pose," in *IEEE Conf. on Computer Vision and Pattern Recognition (CVPR)*, 2018.
- [45] M. Omran, C. Lassner, G. Pons-Moll, P. Gehler, and B. Schiele, "Neural body fitting: Unifying deep learning and model based human pose and shape estimation," *Intl. Conf. on 3D Vision (3DV)*, pp. 484–494, 2018.
- [46] A. Zanfir, E. Marinoiu, and C. Sminchisescu, "Monocular 3D pose and shape estimation of multiple people in natural scenes: The importance of multiple scene constraints," in *IEEE Conf. on Computer Vision and Pattern Recognition (CVPR)*, 2018, pp. 2148–2157.
- [47] V. Ramakrishna, T. Kanade, and Y. Sheikh, "Reconstructing 3D human pose from 2D image landmarks," in *European Conf. on Computer Vision (ECCV)*, 2012.
- [48] C. Wang, Y. Wang, Z. Lin, A. L. Yuille, and W. Gao, "Robust estimation of 3D human poses from a single image," in *IEEE Conf. on Computer Vision and Pattern Recognition (CVPR)*, 2014, pp. 2369–2376.
- [49] J. Cho, M. Lee, and S. Oh, "Single image 3d human pose estimation using a procrustean normal distribution mixture model and model transformation," *Comput. Vis. Image Underst.*, vol. 155, no. C, pp. 150–161, Feb. 2017.
- [50] F. Zhou and F. D. la Torre, "Spatio-temporal matching for human detection in video," in *European Conf. on Computer Vision (ECCV)*, 2014.
- [51] H. Kato, Y. Ushiku, and T. Harada, "Neural 3d mesh renderer," in *IEEE Conf. on Computer Vision and Pattern Recognition (CVPR)*, 2018, pp. 3907–3916.
- [52] D. Lowe, "Distinctive image features from scale-invariant keypoints," *Intl. J. of Computer Vision*, vol. 60, no. 2, pp. 91–110, 2004.
- [53] H. Bay, T. Tuytelaars, and L. V. Gool, "Surf: speeded up robust features," in *European Conf. on Computer Vision (ECCV)*, 2006.
- [54] E. Rublee, V. Rabaud, K. Konolige, and G. Bradski, "Orb: An efficient alternative to sift or surf," in *Intl. Conf. on Computer Vision (ICCV)*. IEEE, 2011, pp. 2564–2571.
- [55] J. Canny, "A computational approach to edge detection," *IEEE Trans. Pattern Anal. Machine Intell.*, vol. 8, no. 6, pp. 679–698, November 1986.
- [56] C. Cadena, L. Carlone, H. Carrillo, Y. Latif, D. Scaramuzza, J. Neira, I. Reid, and J. Leonard, "Past, present, and future of simultaneous localization and mapping: Toward the robust-perception age," *IEEE Trans. Robotics*, vol. 32, no. 6, pp. 1309–1332, 2016, arxiv preprint: 1606.05830, (pdf).
- [57] W. Kim, M. S. Ramanagopal, C. Barto, M. Yu, K. Rosaen, N. Goumas, R. Vasudevan, and M. Johnson-Roberson, "Pedx: Benchmark dataset for metric 3d pose estimation of pedestrians in complex urban intersections," *CoRR*, vol. abs/1809.03605, 2018. [Online]. Available: <http://arxiv.org/abs/1809.03605>
- [58] K. He, G. Gkioxari, P. Dollár, and R. Girshick, "Mask R-CNN," in *Intl. Conf. on Computer Vision (ICCV)*, 2017, pp. 2980–2988.
- [59] X. Zhou, M. Zhu, G. Pavlakos, S. Leonardos, K. G. Derpanis, and K. Daniilidis, "Monocap: Monocular human motion capture using a cnn coupled with a geometric prior," *IEEE Trans. Pattern Anal. Machine Intell.*, vol. 41, no. 4, pp. 901–914, 2018.
- [60] S. Johnson and M. Everingham, "Clustered pose and nonlinear appearance models for human pose estimation," in *British Machine Vision Conf. (BMVC)*, 2010, doi:10.5244/C.24.12.
- [61] C. Lassner, J. Romero, M. Kiefel, F. Bogo, M. J. Black, and P. V. Gehler, "Unite the people: Closing the loop between 3D and 2D human representations," in *IEEE Conf. on Computer Vision and Pattern Recognition (CVPR)*, Jul. 2017.
- [62] C. Ionescu, D. Papava, V. Olaru, and C. Sminchisescu, "Human3.6m: Large scale datasets and predictive methods for 3d human sensing in natural environments," *IEEE Trans. Pattern Anal. Machine Intell.*, vol. 36, no. 7, pp. 1325–1339, Jul 2014.